Transient Thermal Behavior of the Hydration of 2,3-Epoxy-1-propanol in a Continuously Stirred Tank Reactor

ARTICLE *in* INDUSTRIAL & ENGINEERING CHEMISTRY RESEARCH · JANUARY 1996

Impact Factor: 2.59 · DOI: 10.1021/ie00038a008

2 AUTHORS:

Rowena Ball
Australian National University
92 PUBLICATIONS **394** CITATIONS

SEE PROFILE

B. F. Gray
University of Sydney
99 PUBLICATIONS **1,104** CITATIONS

SEE PROFILE

Transient Thermal Behavior of the Hydration of 2,3-Epoxy-1-propanol in a Continuously Stirred Tank Reactor

R. Ball*,† and B. F. Gray‡

School of Chemistry, Macquarie University, North Ryde, New South Wales 2109, Australia, and School of Mathematics and Statistics, University of Sydney, Sydney, New South Wales 2006, Australia

The equations that model a first-order reaction occurring in the four-dimensional parameter space of a CSTR are analyzed using the methods of singularity theory. By reference to experimental data for the hydration of 2,3-epoxy-1-propanol, a direct connection is established between the parameters of the equations and the physical quantities they represent. This simple step suggests a new use for singularity theory as a design tool for chemical reactors, which is illustrated in the latter part of this work by following the pathways of degenerate bifurcations through the codimension 1 and 2 parameter spaces. In the first part of this work, a physical constraint, namely, the boiling point of the reaction mixture, is used to construct a "thermal runaway" curve in the codimension zero operating parameter plane. The shape of this curve reveals the remarkable, but unpleasant, fact that a *decrease* in the ambient temperature can lead to a thermal runaway. Such unexpected and dangerous thermal misbehavior could not be predicted from the classical codimension zero Hopf and saddle–node bifurcation loci.

1. Introduction

The qualitative study of nonlinear ordinary differential equations that model physical processes has been aided by the development of singularity theory (Golubitsky and Schaeffer, 1985), in which bifurcations of successively higher order degeneracy are traced through parameter space to an "organizing center". When appropriate restrictions are placed on the values of the variables and parameters in a dynamical system model, the results of a degenerate bifurcation analysis can assist our understanding of the physical origins of such enigmatic phenomena as steady state multiplicity and oscillations and can predict the onset of this behavior. A systematic method for applying singularity theory to coupled planar systems derived from thermokinetic models was developed by Gray and Roberts (1988a) and has been illustrated by application to a number of simple chemical reaction systems. The Salnikov thermokinetic oscillator (Gray and Roberts, 1988b; Gray and Forbes, 1994), an isothermal chemical reaction scheme (Gray and Roberts, 1988c), and a combustion model (Gray, 1990) have all received the singularity theory treatment, which has uncovered some surprisingly complex behavior for such simple models.

In the present work, we use the methods of Gray and Roberts to analyze a set of coupled ordinary differential equations which model an exothermic reaction occurring in a continuously stirred tank reactor (CSTR). The sequel to the analysis suggests a new application of singularity theory as a design tool for chemical reactors and provides new criteria for the safe operation of such reactors.

The two-dimensional form of the CSTR problem has enduring appeal for the practicing chemical engineer, the laboratory experimentalist, and the theoretician. In all its variants, the model has the general form

$$\dot{x} = X(x,u,\lambda,\rho_1,\rho_2,...,\rho_n) \quad (1)$$

$$\dot{u} = U(x,u,\lambda,\rho_1,\rho_2,...,\rho_n) \quad (2)$$

where X and U are real-valued functions of the variables, the distinguished (bifurcation) parameter λ, and the secondary bifurcation parameters ρ_i. The model possesses the virtues of being directly applicable to real systems while remaining amenable to mathematical treatment.

For the chemical engineer, the spatially homogeneous flow reactor in which a single reactant undergoes a first-order conversion is a practical model of a real problem as well as a useful simplification of systems with more complex chemistry or containing derivatives with respect to space. Since the early work of Denbigh (1971, Chapter 9), efforts have been directed toward specifying design and operating parameters that avoid by a large margin any complex nonlinearities, although this approach has recently been questioned (Seider *et al.*, 1990; Brengel and Seider, 1992; Lewin and Lavie, 1990).

On the theoretical side, the classes of qualitatively distinct behavior of eqs 1 and 2 in the plane of the state variables have been fully described by many workers (Van Heerden, 1958; Bilous and Amundson, 1955; Uppal *et al.*, 1974; Vaganov *et al.*, 1978). The parameter space of the system has also been traversed, according to the principles of singularity theory, with a mathematical outcome of satisfactory elegance, namely, the winged cusp catastrophe (Golubitsky and Keyfitz, 1980; Balakotaiah and Luss, 1983). The bifurcation diagrams which are the results of these and earlier studies of the parameter space (Aris and Amundson, 1958; Hlavacek *et al.*, 1970; Ray and Hastings, 1980) do not translate readily into descriptions of real CSTR states or processes. In these studies, manipulation of the algebraic equations that describe the steady states of the system into analytically tractable form has usually been at the expense of maintaining the experimentally variable quantities as independent parameters. Unlike phase portraits, which faithfully depict the dynamics of a model, the features of a parameter space are not absolute. The presence of objects such as isolas or cusps in a parameter plane or bifurcation diagram depends on which parameters are varied [see, for example, the discussion at the end of the paper by Gray and Roberts (1988b)] or how the system is nondimensionalized. It is felt that this point is not always fully appreciated, and one of the aims of this study is to provide a more

† Macquarie University. E-mail: brian@maths.su.oz.au.
‡ University of Sydney. E-mail: roball@laurel.ocs.mq.edu.au.

0888-5885/95/2634-3726$09.00/0

direct correspondence between the bifurcation parameters of the model and parameters of the real system which can be varied singly and independently by the experimenter.

Laboratory-scale studies of the CSTR have provided valuable evidence for some of the behavior predicted by the model (eqs 1 and 2). The first experimental demonstration of thermal steady state multiplicity in a CSTR used the hydration of 1,2-epoxypropane in acid solution (Furusawa *et al.*, 1969). A series of experiments by Vejtasa and Schmitz (1970), Chang and Schmitz (1975a,b), and Schmitz *et al.* (1979) showed that the oxidation of hydrogen peroxide by thiosulfate ion in a CSTR can occur at two different stable steady states and can also proceed with stable thermal oscillations at certain parameter values. Sustained temperature oscillations were also observed in another experimental system consisting of the acid-catalyzed hydration of 2,3-epoxy-1-propanol to 1,2,3-propanetriol in a CSTR (Heemskerk *et al.*, 1980; Vermeulen and Fortuin, 1986; Vermeulen *et al.*, 1986). Time–temperature measurements for this system agreed well with computed trajectories for one set of experimental conditions. Hysteresis has been documented in the 1,2-epoxypropane hydration reaction (Heemskerk and Fortuin, 1983).

It can be seen from this brief survey that theoretical and experimental advances have taken place in parallel or independently, rather than serially or conjointly. The predictive power of bifurcation analysis has not yet been fully tested against experimental data, nor has its potential to rationalize observed reactor behavior. We shall attempt such a synthesis in this work, by re-examining the published experimental data of Vermeulen *et al.*, mentioned above, using the methods developed by Gray and Roberts for the application of singularity theory. The problem of thermal runaway, which was encountered experimentally in this system, is tackled by applying simple but practical critical damping and thermal runaway conditions and by examining the consequences of the Hopf bifurcation to unstable limit cycles. We then show how the singularity theory approach can provide design and operating specifications for a chemical reactor, by tracing the boundaries of successively higher-order degeneracies through parameter space.

2. Aspects of the Model

In this section, we recapitulate the results of Vermeulen *et al.* and then recast the equations for this system into dimensionless form.

The experimenters measured the transient behavior of the solution phase acid-catalyzed hydration of 2,3-epoxy-1-propanol to 1,2,3-propanetriol, in a cooled CSTR. It was found that the system could settle into sustained thermal oscillations, at a certain value of the coolant inlet temperature, but that it was also prone to thermal runaway, which also seemed to depend on coolant temperature as well as initial conditions. The following equations were found to give an excellent approximation to the experimental data:

$$M\frac{dc}{dt} = -Mcze^{-(E/RT)} + F(c_f - c) \tag{3}$$

$$(MC' + mC'_w)\frac{dT}{dt} = (-\Delta H)cMze^{-(E/RT)} + F(C'_fT_f - C'T) - US(T - T_c) + Q \tag{4}$$

(Some minor changes to the notation used by Vermeulen *et al.* have been made.) Symbols are defined at the end of this paper, as are the dimensionless variables and parameters we have used to reconstruct the above equations in the following form:

$$\frac{dx}{d\tau} = -xe^{((1/\theta)-(1/u))} + f(1 - x) \tag{5}$$

$$\epsilon\frac{du}{d\tau} = \alpha xe^{((1/\theta)-(1/u))} - f(u - \gamma u_f) - l(u - u_c) + q \tag{6}$$

Note that the operating parameters f, u_c, and u_f are fully independent and may be used freely as variable bifurcation parameters, as are the reactor design parameters l and ϵ. There are three categories of parameters: (I) the true constants α, γ, and q, which cannot be varied after the reaction, initial concentration, and stirrer speed are chosen (θ is purely a dimensionless scaling factor); (II) the parameters ϵ and l, which may be varied at the design stage or by structural modification of the reactor [see Schmitz *et al.* (1979) for a method of experimentally varying a parameter equivalent to ϵ]. Practically, it may be necessary to apply restrictions to the physical quantity that is actually varied in these parameters. For example, the solid reactor mass, contained in the parameter ϵ, can be changed without altering the value of l but presumably a change in a quantity such as the heat transfer surface area, contained in l, may concurrently affect ϵ, by affecting the mass; (III) operating parameters f, u_c, and u_f, which may be described as "knobs to twiddle" between or during experiments.

Equations 2 and 3 are best regarded as semiempirical equations that fit the experimental data of Vermeulen *et al.* (1986), although this is not explicitly stated in their work. The reason is that there are no *a priori* grounds for separating the quantities C'_f, the specific heat of the feed, and C', the average specific heat of the reacting mixture, as we have shown in the Appendix. Nevertheless, we have used the original eqs 3 and 4 in the dimensionless forms (5) and (6) for the analysis in section 3 of this work.

3. The Codimension 0 Operating Parameter Plane

In this section we show how the thermal characteristics of the system (eqs 5 and 6) can be summarized in the form of a codimension 0 diagram in the plane of two parameters. Criteria that indicate the likelihood of thermal runaway are also presented in this plane.

The parameter varied experimentally and in numerical simulations by Vermeulen *et al.* was the inlet temperature of the cooling fluid, while the feed temperature was kept constant. Accordingly, we shall use u_c as our principal bifurcation parameter and hold u_f constant. In this section of the analysis we are interested in explaining the observed behavior of a particular system, so we shall declare the only other operating parameter f as a secondary bifurcation parameter. The bifurcation analysis begins with the steady states of the system, defined by

$$X = -xe^{((1/\theta)-(1/u_s))} + f(1 - x) = 0 \tag{7}$$

$$U = [\alpha xe^{((1/\theta)-(1/u_s))} - f(u_s - \gamma u_f) - l(u_s - u_c) + q]/\epsilon = 0 \tag{8}$$

The Jacobian matrix of the differential coefficients of the linearization is formed, which in terms of eqs 7 and

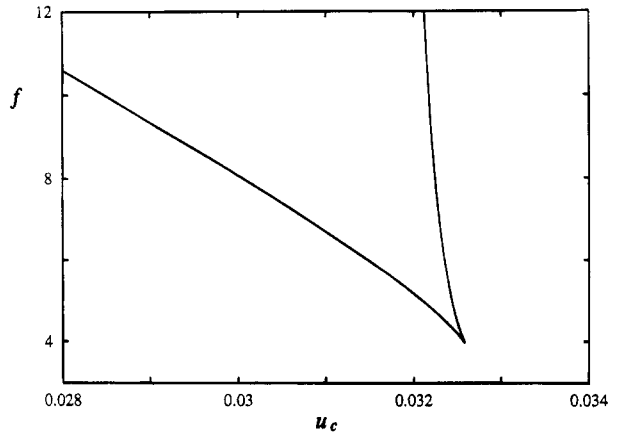

Figure 1. Codimension 0 saddle–node curve in the u_c–f parameter plane. Other parameters: $\epsilon = 1.53$, $l = 22.9$, $u_f = 0.0310$, $\alpha = 0.0339$, $\gamma = 1.11$, and $q = 0.00265$.

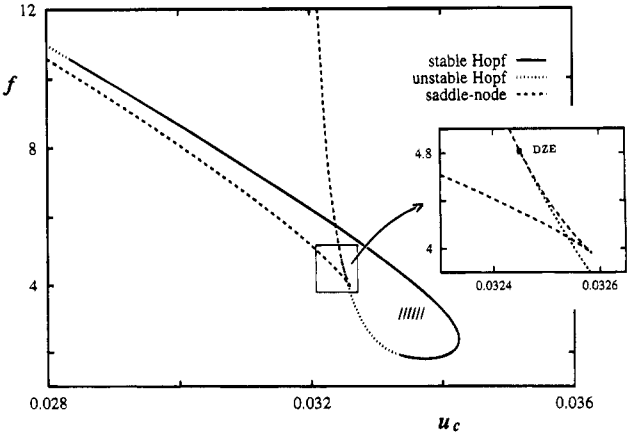

Figure 2. Codimension 0 Hopf and saddle–node curves in the u_c–f parameter plane. Other parameters as for Figure 1.

8 is

$$J = \begin{bmatrix} -e^{((1/\theta) - (1/u_s))} - f & \dfrac{-\alpha e^{((1/\theta) - (1/u_s))}}{u_s^2} \\ \dfrac{\alpha e^{((1/\theta) - (1/u_s))}}{\epsilon} & \left(\dfrac{\alpha\gamma e^{((1/\theta) - (1/u_s))}}{u_s^2} - f - l\right)/\epsilon \end{bmatrix} \quad (9)$$

The codimension zero steady state bifurcation is the saddle–node, which is defined by eqs 7 and 8 and the condition

$$\det J = 0 \quad (10)$$

as well as the appropriate nondegeneracy conditions.

Numerical roots to eqs 7, 8, and 10 for a range of the temperature variable u_s define a locus in the u_c–f parameter plane which is plotted as the codimension 0 saddle–node curve in Figure 1. This boundary heralds the emergence (or disappearance) of two more solutions to eqs 7 and 8: a saddle and a node or focus. The cusp is the only codimension 1 steady state degeneracy in this section of the plane; it is called the hysteresis point and represents the coalescence of the two limit points in the u_c–u_s plane.

Oscillatory solutions to eqs 5 and 6 may appear via the Hopf bifurcation, which is defined (for the two-dimensional case) by the steady state eqs 7 and 8, and the additional conditions

$$\operatorname{tr} J = 0 \quad (11)$$

$$\left.\begin{aligned} \det J &> 0 \\ \frac{d(\operatorname{tr} J)}{d\lambda} &\neq 0 \\ u_2 &\neq 0 \end{aligned}\right\} \quad (12)$$

The symbol λ represents either u_c or f, whichever we choose as the distinguished parameter. The above defining and nondegeneracy conditions have been treated rigorously in many references [a comprehensive discussion of the Hopf bifurcation can be found in Marsden and McCracken (1976)]. In the present context, the nondegeneracy conditions (12) may be interpreted geometrically by reference to Figure 2, in which the locus of Hopf bifurcations, obtained numerically from eqs 7, 8, and 11, has been superimposed upon the saddle–node curve of Figure 1. The degenerate points that occur when one or more of the above conditions are breached may be tracked through a parameter space of higher dimensionality. In section 4 we shall travel with these points through the codimension 1 and 2 parameter spaces.

The double-zero eigenvalue (DZE) point in Figure 2 punctuates the transition of the characteristic eigenvalues from complex conjugate to real. As this point is crossed along the Hopf curve, the corresponding steady state with its incipient limit cycle undergoes a switch in stability as det J passes through zero. The Hopf curve ends here because the eigenvalues are real where tr $J = 0$. Two $H2_1$ points (Gray and Roberts, 1988a) also occur on the Hopf curve; geometrically, they simply mark the extreme values of the bifurcation parameters for the occurrence of limit cycles in the phase plane. Along the curve, the stability of the bifurcating limit cycle is determined by the sign of the coefficient μ_2 of the second-order term in the Taylor series expansions of eqs 7 and 8. For $\mu_2 < 0$ the limit cycle evolves stably and attracts all nearby trajectories in phase space onto itself, and for $\mu_2 > 0$ an unstable limit cycle will evolve and direct nearby trajectories away from itself. The points at which $\mu_2 = 0$ in Figure 2 represent the occurrence of two $H3_1$ degeneracies [critical Hopf bifurcations; see Gray and Roberts (1988a)]. The locations of these points have been calculated numerically from the formula given by Andronov (1973).

Two nonlocal intersections of the Hopf and saddle–node curves represent parameter values at which a lower Hopf bifurcation coincidentally concurs with an upper limit point, on the steady state curve, and an upper Hopf bifurcation with a lower limit point. The intersections are nonlocal because the coincident Hopf and limit points occur at different temperatures.

The small hatched area in Figure 2 represents the region in which the reactor was experimentally operated, while the Hopf and saddle–node curves give the ranges of operating parameter values for which steady state multiplicity and autarkical oscillations may be expected. But we are also interested in the problem of thermal runaway encountered by the experimenters, about which Figure 2, as it stands, gives us no information. In a liquid phase system one would expect a critical, possibly explosive, situation to develop if the reactor temperature were to reach or exceed the boiling point of the reaction mixture. A desired steady state that is thermally stable may never be achieved if the transient makes a large excursion to a dangerously high temperature, before spiraling into the (theoretically) stable steady state or limit cycle. An example of such a

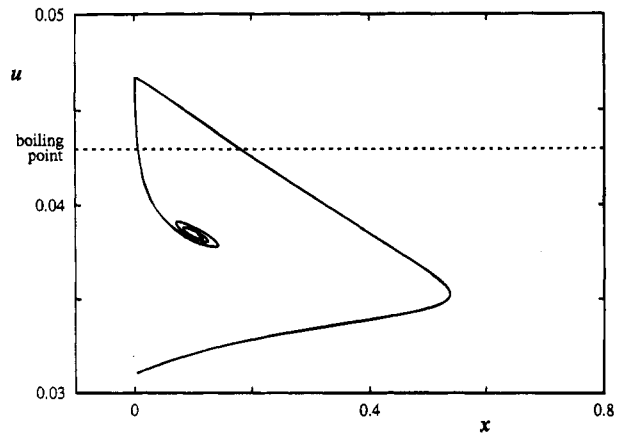

Figure 3. Phase portrait showing how a large temperature excursion on a spiral trajectory can lead to a thermal runaway. Parameters: $f = 4.0$, $u_c = 0.0337$; other parameters as for Figure 1.

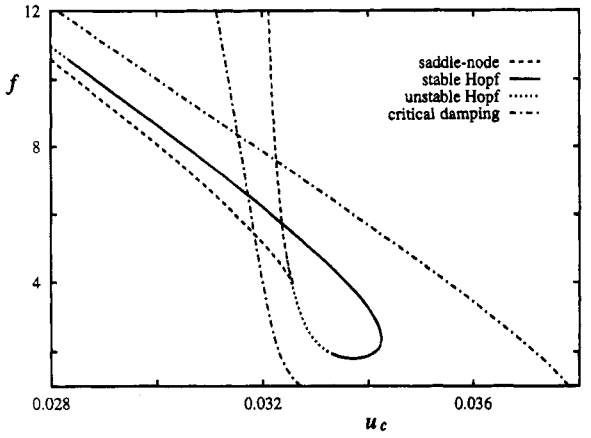

Figure 4. Codimension critical damping, Hopf, and saddle–node curves in the u_c–f parameter plane. Other parameters as for Figure 1.

spiral trajectory is shown in the phase portrait of Figure 3. A facile and circumspect condition for the onset of this behavior in the reactor would signal a change in the qualitative character of the steady state in the phase plane from node to focus. This occurs when

$$(\mathrm{tr}\, J)^2 - 4 \det J = 0 \tag{13}$$

We have termed this the critical damping condition, by analogy with mechanical and electrical systems. (In thermochemical systems the analogue of a mechanical or electrical damping force is the heat loss rate, $l(u - u_c)$. To our knowledge this is the first time the condition (eq 13) has been applied to a chemical system.) The loci of u_c, f points, which simultaneously satisfy eqs 7, 8, and 13, are plotted in Figure 4, superimposed on the Hopf and saddle–node curves of Figure 2.

Two questions arise when we consider the practical value of the critical damping curves of Figure 4. First, is the operation of the reactor *outside* the critical damping region in Figure 4 a guarantee of docile thermal behavior, in view of the fact that spiral trajectories such as that in Figure 3 are obtained at parameter values *inside* this region? Second, is there a parameter region between the spiral curves within which the reactor may still be operated with an acceptable margin of safety? To answer these questions, we seek values of u_c and of f for which the maximum transient temperature u is less than u_b, the boiling point of the reaction mixture:

$$u_{max} < u_b \tag{14}$$

This is another condition that, like the thermal runaway condition, is topologically inconsequential but practically useful. There is no steady state condition to be applied here. The value of u is monitored along numerically computed solution curves to the dynamic eqs 5 and 6, for a given set of initial conditions and a range of u_c and f values. Normally, the reactor would be started up with $x = 0$ (water only in the reactor) and $u = u_f$, the feed temperature. With these starting conditions, the u_c, f pairs for which $u_{max} = u_b$ form the thermal runaway curve in Figure 5, superimposed on the saddle–node, Hopf, and critical damping curves of Figure 4. Note that the thermal runaway curve ap-

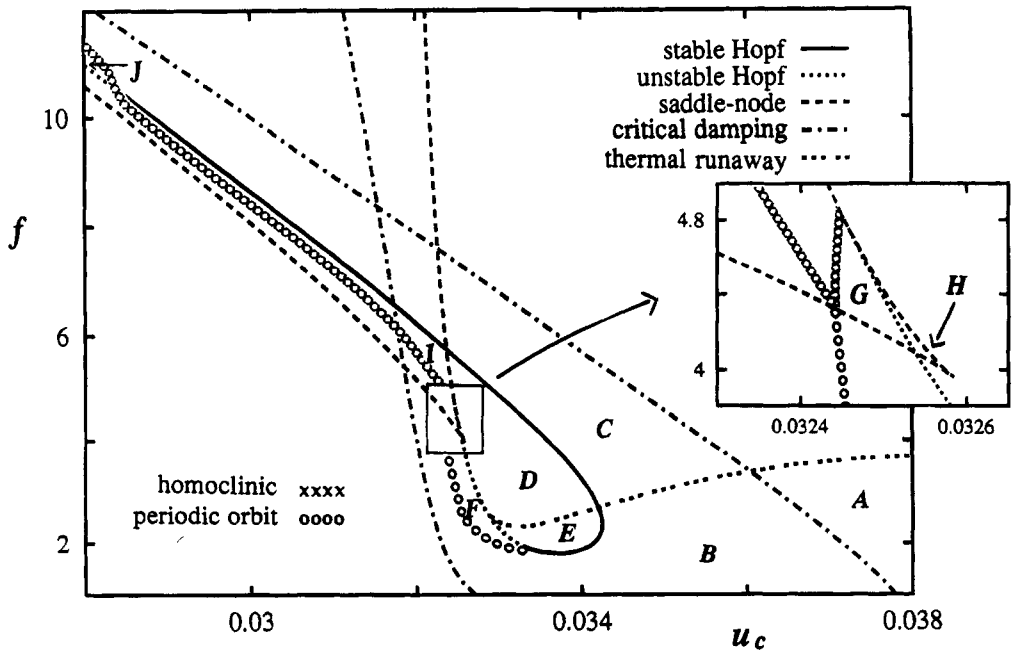

Figure 5. Completed codimension 0 diagram in the u_c–f parameter plane. Other parameters as for Figure 1. The labels A–J refer to the phase portraits of Figure 7.

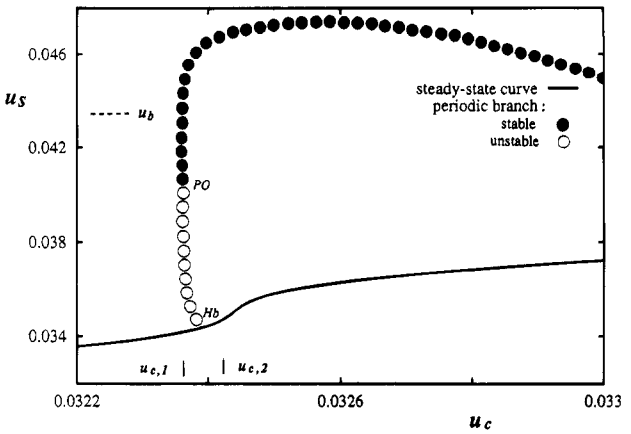

Figure 6. Bifurcation diagram illustrating the possible thermal consequences of the periodic orbit bifurcation. Parameters: $f = 3.3$, $l = 20$; other parameters as for Figure 1.

proaches and then coincides (numerically) with the lower part of the Hopf curve and the upper arm of the saddle–node curve. It can also be seen that the critical damping curve, in this instance, is largely benign, in the sense that it does not correlate well with the thermal runaway curve.

Two more curves of bifurcations have been drawn in Figure 5. These are the periodic orbit and homoclinic curves. Their exact positions have not been computed numerically. Qualitative arguments give their approximate locations. On a bifurcation diagram, a homoclinic point indicates termination of a branch of periodic solutions in an infinite periodic orbit. The curves of such points in the codimension 0 plane begin at a DZE point and end on the saddle–node curve, coinciding with the periodic orbit juncture. The latter bifurcation occurs at the switch in stability of a branch of limit cycles at a turning point, as shown in the bifurcation diagram of Figure 6. The codimension 0 curve of these points begins at an $H3_1$ point and, in this case, ends on the saddle–node curve. It is discussed more fully below, in terms of the implications for thermal stability.

Let us now traverse a path around this parameter plane, pausing before we cross each boundary to view the transient and steady states of the reactor in the phase plane. Each of the labeled regions in Figure 5 has a corresponding phase portrait in Figure 7. [We have chosen not to draw each of the qualitatively distinct phase portraits of the system (eqs 5 and 6). All 35 of them have been given, in stylized form, by Vaganov *et al.* (1978). We have selected instead from Figure 5 those phase portraits which pertain, in a practical sense, to the control of the system under study.] Region A is thermally safe. So is region B,

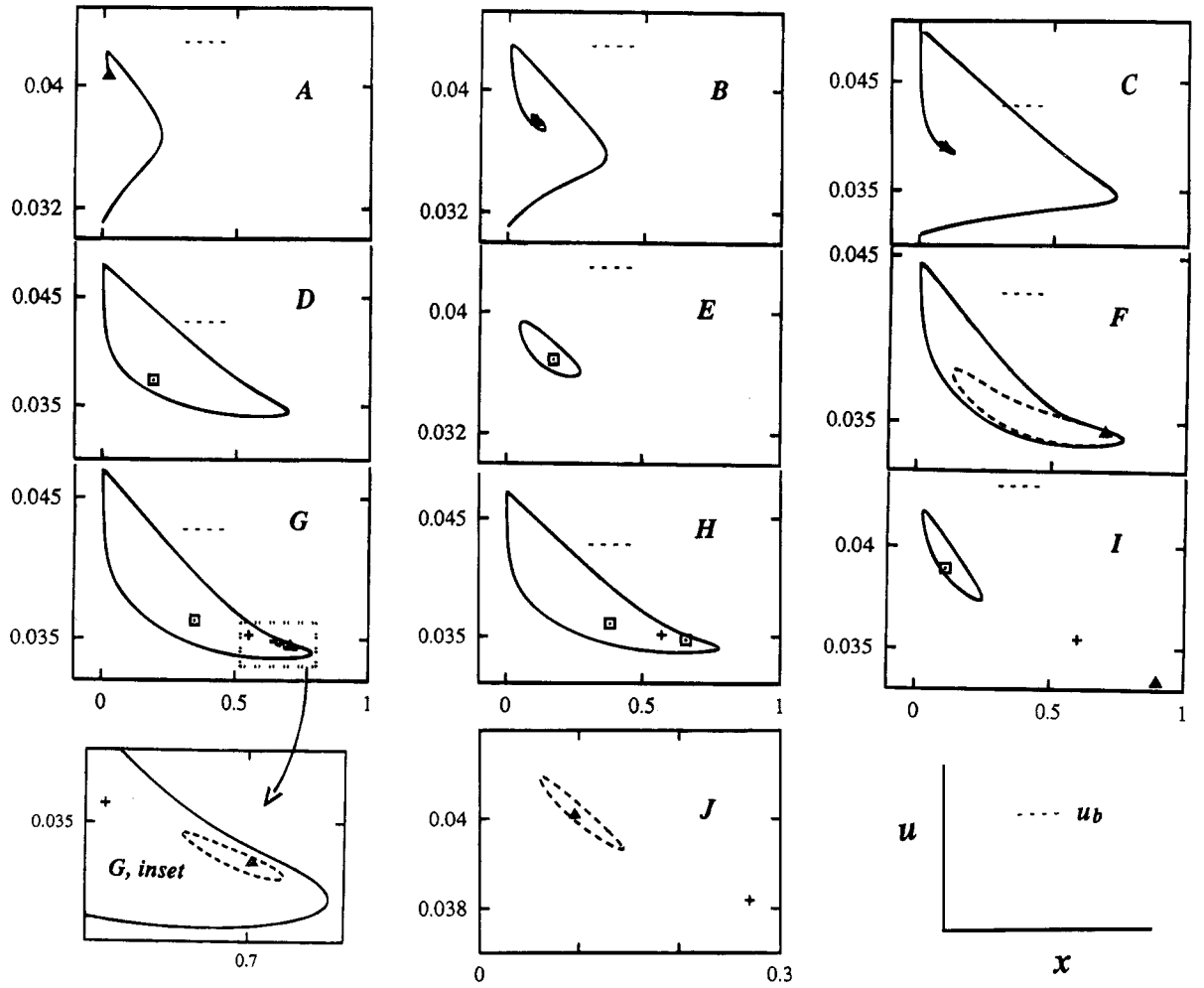

Figure 7. Phase portraits from the regions A–J in Figure 5. Other parameters as for Figure 1. Parameters:

	A	B	C	D	E	F	G	H	I	J
f	3.0	2.8	4.0	4.0	2.5	3.8	4.2	4.1	6.0	10.985
u_c	0.037	0.03345	0.0337	0.0328	0.034	0.0325611	0.03252	0.03255	0.03208	0.028

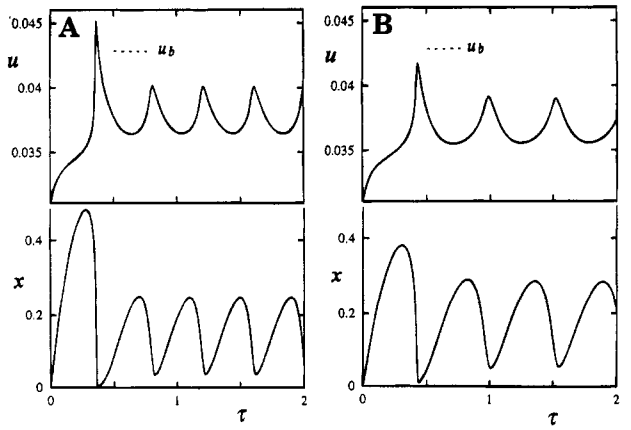

Figure 8. Temperature and concentration transients of the integrated eqs 5 and 6. (A) $f = 2.2$, $u_c = 0.0341$; (B) $f = 3.3$, $u_{-c} = 0.0338$; other parameters as for Figure 1.

although the transient traces out a shrinking helix inside an envelope of exponential decay. As we cross the thermal runaway curve into region C, we encounter the remarkable phenomenon observed by Vermeulen *et al.* in a simulation: a *decrease* in the coolant temperature, at constant flow rate, can lead to thermal runaway. This fact is so counterintuitive that we do not hesitate to call this the most practically important curve in the codimension 0 plane. A naive and spontaneous maneuver by an operator to control the damped oscillations in region B, which may be deemed thermally hazardous or otherwise undesirable, may be to run out the reactant and then restart the reactor at a lower coolant temperature. At constant flow rate, according to Figures 5 and 7C, this could be disastrous. In an actual operational situation, where there may be random, accidental, or intentional fluctuations in u_c, the starting conditions for any thermal excursion are not $x = 0$, $u = u_f$ as used above, but rather $x = x_s$, $u = u_s$. Numerical computations of thermal runaway curves for a number of sets of perturbed steady state "initial conditions" have shown that the general shape and position of the curves are similar to that in Figure 5.

The phenomenon of increasing reactor temperature excursions with decreasing ambient temperature may not be unusual in flow systems. It has been observed experimentally in the $H_2 + Cl_2$ reaction in a semibatch reactor, and been simulated in the liquid phase $H_2O_2 + Na_2S_2O_3$ reaction, also under semibatch conditions (Gray *et al.*, 1993). Some clues to the physical origins of this behavior may be obtained from the time series in Figure 8. It appears that the extent to which reactant can accumulate determines the potency of the autocatalytic effect of heat release as conversion proceeds and establishes the phase lag between concentration and temperature extrema. At this stage, we cannot predict whether it is a general phenomenon or whether there may be a characteristically susceptible reaction system.

In region D of Figure 7, the predicted convergence to a large-amplitude stable limit cycle would never eventuate in practice from normal starting conditions, again because u exceeds u_b before the trajectory converges to the limit cycle. (As intimated above, it should be kept in mind that there is a different thermal runaway bifurcation curve for each set of initial conditions. We have presented only one such curve here.) Passing into region E, there are stable thermal oscillations where the maximum temperature remains lower than u_b. Just to the left of the Hopf curve, region F is a narrow strip in which the phase portrait has a stable steady state surrounded by an unstable limit cycle, which in turn is surrounded by a stable limit cycle. The periodic orbit bifurcation occurs at the coalescence of these two limit cycles and may be a source of thermal instability. Its presence may result in the abrupt appearance or extinction of large-amplitude oscillations as u_c is varied about the bifurcation value. This is illustrated by reference to Figure 6. The coolant temperature u_c is not necessarily under fine control; more likely, it is subject to ambient fluctuations. Under these circumstances, a drift from, say, $u_{c,1}$ to $u_{c,2}$ in Figure 6 may be accompanied by a jump to the temperature peak of a large-amplitude oscillation.

Crossing the lower arm of the saddle–node curve we enter the region of threefold multiplicity. This region is subdivided into several smaller areas, owing to the close approach of the Hopf, saddle–node, homoclinic, and periodic orbit curves. Phase portraits for these and the other labeled regions of Figure 5 are given in Figure 7. Most of the area of multiplicity, between the arms of the saddle–node curve, is on the safe side of the thermal runaway curve (as pointed out above, this curve coincides numerically with the upper arm of the saddle–node curve). This fact raises interesting, and hitherto unexplored, possibilities for optimizing reactor operation. For instance, there appears to be a thermally safe state of high conversion and a safely accessible state of low conversion which may be used to start or quench the reaction.

Finally, we note briefly the second change in stability of the Hopf curve at low u_c and high f. In this system, the upper $H3_1$ degeneracy is of no thermal consequence, but its presence may have significance in other systems.

4. Designing a Reactor Using Bifurcation Analysis

In this section we introduce the reactor design parameters ϵ, which describes the solid mass of the reactor, and l, which describes the degree of heat transfer to the coolant, as bifurcation parameters. We demonstrate how a reactor may be designed for a chosen reaction by examination of the higher codimension parameter space.

4.1. Prelude. The interesting thermal behavior of the 2,3-epoxy-1-propanol → glycerol system treated in the previous section makes it a suitable subject for this analysis. We wish to illustrate the essential features of the method and of the results without carrying superfluous terms or parameters, so from eqs 4 and 5 we shall discard explicitly the small work term q and allow the ratio γ to equal 1 (we have justified this theoretically in the Appendix). The equations so modified are

$$\frac{dx}{d\tau} = -xe^{((1/\theta)-(1/u))} + f(1-x) \tag{15}$$

$$\epsilon\frac{du}{d\tau} = \alpha xe^{((1/\theta)-(1/u))} - f(u-u_f) - l(u-u_c) \tag{16}$$

In the steady state, these combine to the bifurcation equation

$$\mathcal{F} = \frac{\alpha f e^{((1/\theta)-(1/u_s))}}{(e^{((1/\theta)-(1/u_s))}+f)} - f(u_s-u_f) - l(u_s-u_c) = 0 \tag{17}$$

Now we shall expand our field of view from the simple exploration of the operating parameter plane in the previous section and consider our analytic brief to be

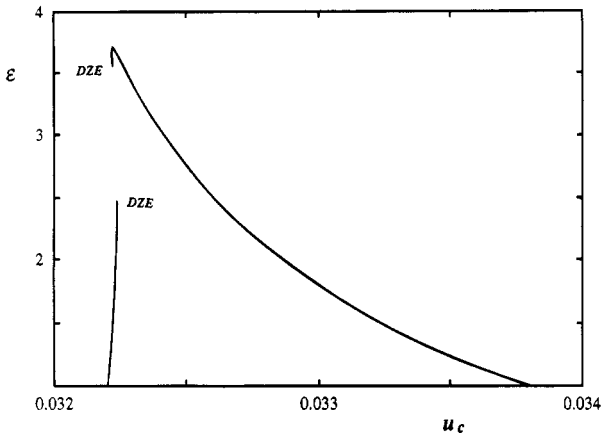

Figure 9. Codimension 0 Hopf curve in the u_c–ϵ parameter plane. Parameters: $l = 18.5$, $f = 3.3$, $u_f = 0.031$, and $\alpha = 0.034$.

the total design and operating parameter space. The principal bifurcation parameter remains u_c, but thereafter we change the direction in which we traverse the parameter space and choose ϵ as the next bifurcation parameter. Then the other design parameter l will be varied, and finally the flow rate f.

4.2. The Analysis. Notice, from eq 16, that ϵ is a "transient" parameter, in that it affects the transient and oscillatory behavior but not the steady states. The dynamic effects of a parameter equivalent to ϵ have been studied experimentally by Chang and Schmitz (1975a), as noted in section 2, and theoretically by Hlavacek *et al.* (1970). In the u_c–ϵ parameter plane the basic codimension zero curve is the Hopf locus. The defining and nondegeneracy conditions described above yield equations in parametric form for the curve of Hopf bifurcations, parameterized by the steady-state temperature, u_s:

$$u_c = \frac{1}{l}\left[\frac{-\alpha f e^{((1/\theta)-(1/u_s))}}{(e^{((1/\theta)-(1/u_s))}+f)} + f(u_s - u_f) + l u_s\right] \quad (18)$$

$$\epsilon = \frac{1}{(e^{((1/\theta)-(1/u_s))}+f)}\left[\frac{\alpha f e^{((1/\theta)-(1/u_s))}}{(e^{((1/\theta)-(1/u_s))}+f)} - f - l\right] \quad (19)$$

This curve is plotted in Figure 9, for chosen values of l and f. We see at once that there is a critical solid mass capacitance above which oscillations arising from Hopf bifurcations cannot occur. This is the $H2_1$ point in Figure 9. Also featured are the two DZE points: they inform us that the system is capable of steady state multiplicity, although direct information concerning steady state bifurcations is not contained in this diagram. In fact, it is not necessary, as we shall shortly demonstrate.

The next parameter to be varied is l, another design parameter, which is a measure of the efficiency of heat transfer to the coolant. The degeneracies in the codimension 0 diagram may now be unfolded into codimension 1 diagrams. Parametric equations for the $H2_1$ and DZE loci are obtained after selection of the appropriate conditions from the Hopf defining conditions of eqs 11 and 12 and the steady state condition of eq 17. For $H2_1$ degeneracies

$$l = \frac{\alpha f}{u_s^2(e^{((1/\theta)-(1/u_s))}+f)}[e^{((1/\theta)-(1/u_s))}(1+2u_s) - f(1-2u_s)] - f \quad (20)$$

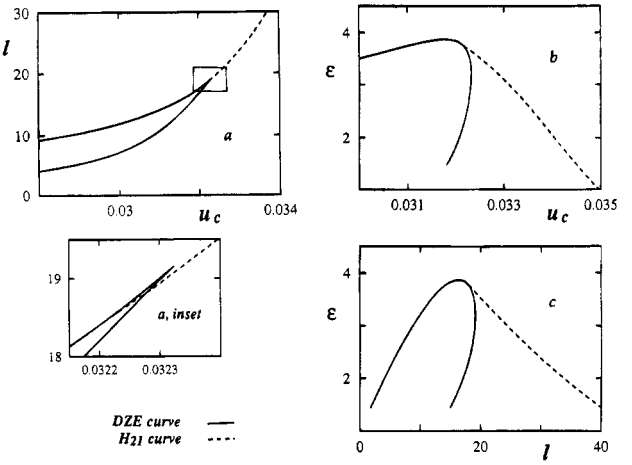

Figure 10. Codimension 1 curves in the u_c–ϵ–l parameter space. Parameters: $f = 3.3$, $u_f = 0.031$, and $\alpha = 0.034$.

$$\epsilon = \frac{\alpha f^2}{u_s^2(e^{((1/\theta)-(1/u_s))}+f)^2}\left[1 - \frac{2u_s e^{((1/\theta)-(1/u_s))}}{f} - 2u_s\right] \quad (21)$$

with u_c defined by using eq 20 in eq 18. For DZE degeneracies

$$l = \frac{\alpha f^2 e^{((1/\theta)-(1/u_s))}}{u_s^2(e^{((1/\theta)-(1/u_s))}+f)^2} - f \quad (22)$$

$$\epsilon = \frac{\alpha f e^{((2/\theta)-(2/u_s))}}{u_s^2(e^{((1/\theta)-(1/u_s))}+f)^3} \quad (23)$$

with u_c defined by using eq 22 in eq 18.

Figure 10a displays the curves of these codimension 1 bifurcations in the $u_c - l$ parameter plane. The DZE curve is also the codimension zero saddle–node curve because eqs 22 and 18 also satisfy the saddle–node bifurcation conditions $\det J = 0$, $\mathcal{G} = 0$. This fact enables us to keep track of the steady state bifurcations without losing the essential dynamical information provided by varying the parameter ϵ. Of course, the $H2_1$ and the DZE curves may also be presented in the u_c–ϵ or l–ϵ planes; indeed, our analysis of the parameter space is greatly assisted by doing so, and these are presented in Figure 10b,c. The abrupt ends of the DZE curves in Figure 10b,c represent the limits of the physical parameter space (all parameters are defined only for λ, $\rho_i \geq 0$).

The paths taken by the $H2_1$ and DZE curves lead to the codimension 2 degeneracies. At least one more parameter must be varied to unfold these degenerate points. Obviously, this should be f, the second operating parameter. The point of intersection in parts a–c of Figure 10 is an $H2_1$–DZE degenerate bifurcation. It is unfolded by forming a parametric equation in f from the appropriate defining conditions,

$$f = \frac{e^{((1/\theta)-(1/u_s))}}{2(1-2u_s)}[(4u_s - 1) + (5 - 8u_s)^{1/2}] \quad (24)$$

and using this in eqs 18, 22, and 23. The unfolded curve of $H2_1$–DZE points is projected onto the six possible parameter planes in Figure 11.

Returning to Figure 10a, there is another degeneracy that we have not yet unfolded. This, the cusp in Figure 10a, is the codimension 2 DZE–DZE degeneracy. The

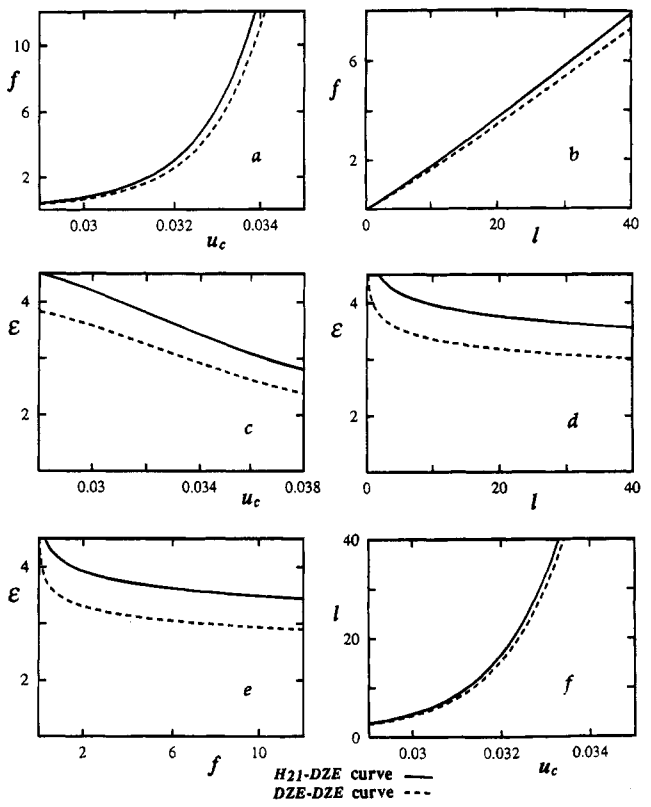

Figure 11. Codimension 2 DZE−DZE and $H2_1$−DZE curves in u_c−ϵ−l−f parameter space: $u_f = 0.031$ and $\alpha = 0.034$.

extra bifurcation condition is

$$\mathscr{G}' = 0 \tag{25}$$

which yields the parametric equation for f

$$f = e^{((1/\theta)-(1/u_s))}\frac{(1 + 2u_s)}{(1 - 2u_s)} \tag{26}$$

Using this in eqs 18, 22, and 23 we obtain the curve of DZE−DZE bifurcations which we have plotted with the $H2_1$−DZE curve in the parameter planes of Figure 11. A search for codimension 3 degenerate points does not seem warranted at this stage. For instance, the values of u_s which satisfy eqs 24 and 26 simultaneously are unphysical or impracticable in the system under study.

Let us return momentarily to the codimension 0 parameter space of Figure 9, and recall, from the discussion in section 3, that a decrease in the coolant temperature can trigger a large thermal excursion. In the interests of safe reactor design it may be useful to view the thermal runaway curve, which is the curve of points for which $u = u_b$ (with the initial conditions $x = 0$, $u = u_f$), in the u_c−ϵ parameter plane and ascertain its persistance on variation of f or l. In Figure 12a this curve has been superimposed on a codimension 0 Hopf curve. Critical points on the thermal runaway curve, such as the maximum, could be tracked, with some labor, through the parameter space, but it is probably more illustrative to remain on the u_c−ϵ plane and draw the curve for several values of l and f, as in Figure 12. Again it can be seen that a decrease in the coolant temperature can result in an increase in reactor temperature. Evidently this kind of thermal misbehavior is a characteristic of the reaction system as a whole, at least over the region of parameter space covered by Figure 12.

4.3. Discussion. Here is a simple demonstration of how the diagrams of Figures 10−12 may be used to design a chemical reactor in which to carry out the hydration of 2,3-epoxy-1-propanol. First, we shall try designing a reactor in which there is no possibility of Hopf bifurcations or multiple steady states for any values of the operating parameters. Economic considerations may dictate a rather small cooling capacity, so the value of 15 is chosen for l. From Figure 11d, ϵ must be at least 3.8 if reactor operation is to be confined to the region above the $H2_1$−DZE curve. Moving to Figure 11c, one can see that the coolant temperature must be >0.032, while from Figure 11a,b the maximum flow rate is 3. If we are allowed a larger surface area for heat exchange, such that $l = 26$, then the minimum allowable value of ϵ is reduced only a little, to 3.7, while u_c must be higher. We are forced to concede that a reactor in which oscillations and multiplicity are precluded by design is an impracticable proposition, if it is difficult to achieve a large solid thermal capacitance.

In practical terms then, the parameter space of the reactor is probably the lower region of Figure 11d, and there will be Hopf bifurcations and multiplicity for some range of u_c, f, and l. Our task is now to fine tune the parameters so that no Hopf bifurcations appear on the steady state curve, or if they do, to ensure that the reactor can be operated at a sufficient distance from them. If the minimum flow rate is set, we can return to the codimension 1 space. In the codimension 1 plots of Figure 10, the flow rate is set at 3.3. One can see that the value of ϵ can be reduced to a more realistic level—2.8, say—and the oscillatory and multiplicity regions can still be avoided, provided $u_c > 0.0335$ and $l > 26$. From Figure 12, this set of parameter values also places the reactor safely outside the region where $u > u_b$.

The codimension 1 and 2 diagrams of Figures 10 and 11 are greatly simplified, because they are intended only for illustrating the general approach for using bifurcation analysis in reactor design. For any given brief, a more thorough exploration of the codimension 1 and 2 parameter spaces may be necessary. Ideally, one would trace degeneracies that involve homoclinic, $H3_1$, and periodic orbit bifurcations through to codimension 2. The computational effort required would be rather forbidding, so it is probably easier to regard the diagrams of Figures 10 and 11, obtainable from parametric equations, as design tools from which a provisional set of parameters can be obtained. The bifurcation diagram can then be constructed, and the positions of features such as homoclinic termini and switches of stability noted.

In view of the discussion in section 3, we certainly also wish to build transient thermal safety into the reactor design. As pointed out above, it is computationally rather laborious to follow degeneracies in the thermal runaway curve through codimension 1 space and beyond. To this extent, transient thermal misbehavior cannot be excluded from a reactor design at the outset. A thermal runaway curve can be constructed in a u_c−ρ_i plane once the reactor design has been chosen, as in Figure 12 and Figure 5 of section 3. Knowledge of the shape of this curve is essential in both the design and operation of a reactor.

The design process may also be turned around. Practicality may dictate that the reactor be operated with a coolant temperature corresponding to room temperature and a feed flow rate that is constrained

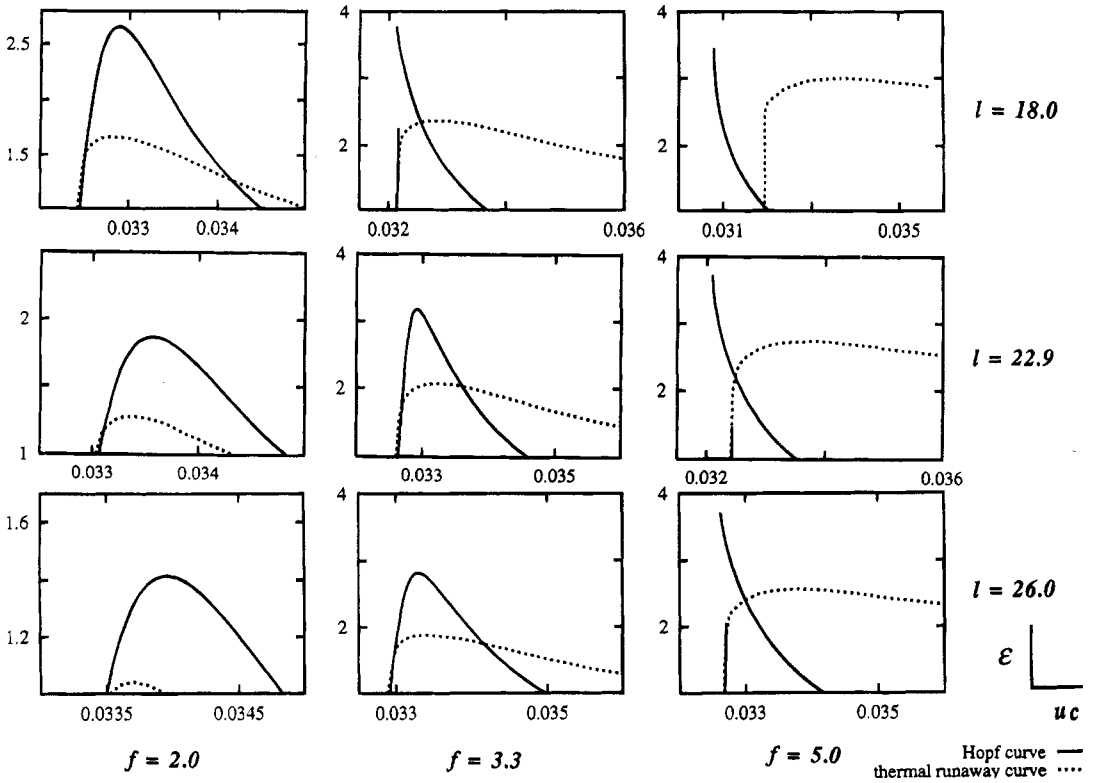

Figure 12. Some examples of thermal runaway curves, superimposed on corresponding Hopf curves, in the u_c–ϵ plane, for various values of l and f: $u_f = 0.031$ and $\alpha = 0.034$.

by the rates of preceding or succeeding processes (such as separation of the product) or by a specified degree of conversion. Accordingly, u_c and f are fixed at 0.031 and 3.3, respectively. Again consulting Figure 10, for any realistic ϵ (<2.8), this places the reactor squarely in the region of multiplicity, unless we can arrange for l to be greater than 18.

5. Conclusions

1. Application of bifurcation theory to the CSTR in practical circumstances requires the use of independently variable parameters that correspond to physical quantities in the system.

2. The volumetric heat capacity of the reaction mixture is adequately described by a single quantity, when the first-order approximation is made that the heat capacity is independent of temperature.

3. A codimension 0 parameter plane curve that defines the onset of critical damping in the phase plane is useful for elucidating transient thermal behavior in the CSTR.

4. For the acid-catalyzed hydration of 2,3-epoxy-1-propanol in a CSTR, a thermal runaway curve is constructed which shows that a decrease in the ambient temperature can result in a thermal runaway.

5. Singularity theory can be used as a chemical reactor design tool, in conjunction with appropriate numerical computations of transient states and bifurcation loci.

Nomenclature

c = concentration of reactant (mol kg^{-1}, mol L^{-1})
C = molar heat capacity (J mol^{-1} K^{-1})
C' = average specific heat capacity of mixture in the reactor (eq 4) (2.50 × 10^3 J kg^{-1} K^{-1})
C_f' = specific heat capacity of feed mixture (2.77 × 10^3 J kg^{-1} K^{-1})
$\bar{C}$ = volumetric heat capacity of feed mixture (eq 38) (J L^{-1} K^{-1})
E = activation energy (73.4 kJ mol^{-1})
h = enthalpy content
ΔH = reaction enthalpy (−87.7 kJ mol^{-1})
J = the Jacobian matrix (eq 9)
mC_w = specific heat of solid parts of the reactor (J K^{-1})
M = total mass of reaction mixture (0.300 kg)
Q = rate of heat generation by mixing and stirring (33.4 W)
R = gas constant (8.314 J mol^{-1} K^{-1})
S = surface area of cooling coil available for heat transfer (m^2)
t = time (s)
T = temperature (K)
U = heat transfer coefficient of the cooling coil (W m^{-2} K^{-1})
V = reactor volume (L)
z = pseudo-first-order frequency factor (1.35 × 10^{10} s^{-1})

Dimensionless Variables and Parameters

$f = F/Mze^{-(1/\theta)}$
$l = (US)/(C'Mze^{-(1/\theta)})$
$q = (QR)/(Mze^{-(1/\theta)}EC')$ (0.00265)
$u = (RT)/E$
$x = c/c_f$
$\alpha = (Rc_f(-\Delta H))/(C'E)$ (0.0339)
$\gamma = C_f'/C'$ (1.11)
$\epsilon = (MC' + mC_w)/(MC')$
θ = dimensionless scaling factor (0.0338)
$\tau = tze^{-(1/\theta)}$

Other Symbols

$\mathscr{G}$ = function defined in eq 17
U = generalized function in eq 1, defined in eq 8
X = generalized function in eq 1, defined in eq 7
λ = principal bifurcation parameter

μ_2 = coefficient of the second-order term in the Taylor series expansions of eqs 7 and 8
ϕ = an eigenfunction
ρ = a secondary bifurcation parameter

Subscripts

b = of the mixture boiling point
c = of the coolant
f = of the feed
p = at constant pressure, of the product
r = of the reactant
s = of the steady state, of the solvent (in the Appendix only)

Abbreviations

det J = the determinant of the Jacobian matrix
DZE = double-zero eigenvalue
tr J = the trace of the Jacobian matrix

Appendix

As intimated in section 2, there is no theoretical requirement in the CSTR model for separate quantities C_f' and C'. To show why this is so, we must begin with a fundamental enthalpy balance for the first-order reaction in a CSTR. (Following the principle of Occam's razor, we have shed unnecessary encumbrances. For pedagogical purposes the reactor is made adiabatic, and the terms representing the solid mass capacitance and the small constant rate of work done on the reaction mixture are omitted. The reaction mixture volume has been used in preference to the mass—the choice is purely a matter of convention, and obviously other units must be chosen with consistency.)

$$V\frac{d}{dt}[ch_r(T) + (c_f - c)h_p(T) + c_s h_s(T)] = F[c_f h_r(T_f) - ch_r(T) - c_s h_s(T) - (c_f - c)h_p(T)] \quad (27)$$

where the notation $h_r(T)$, etc., indicates the temperature dependence of the enthalpy of each species. Differentiating the left-hand side of eq 27 and making use of the thermodynamic relation

$$C_p = \left(\frac{\partial h}{\partial T}\right)_p \quad (28)$$

we obtain the rate of enthalpy change in the reactor in terms of concentrations, molar heat capacities, and the temperature:

$$V[(h_r - h_p) + (cC_{p,r} + (c_f - c)C_{p,p} + c_s C_{p,s})]\frac{dT}{dt} = F[c_f h_r(T_f) + c_s h_s(T_f) - ch_r - c_s h_s - (c_f - c)h_p] \quad (29)$$

where now, for brevity, only the dependence of the enthalpy on the feed temperature is explicitly indicated. The relation (28) yields the first-order approximations

$$h_r(T_f) - h_r = C_{p,r}(T_f - T), \quad h_s(T_f) - h_s = C_{p,s}(T_f - T) \quad (30)$$

We also need the mass conservation equation

$$V\frac{dc}{dt} = -Vzce^{-(E/RT)} + F(c_f - c) \quad (31)$$

By substituting eqs 30 and 31 into eq 29 and rearranging, we obtain

$$V[cC_{p,r} + (c_f - c)C_{p,p} + c_s C_{p,s}]\frac{dT}{dt} = -(h_p - h_r)Vzce^{-(E/RT)} + F(c_f C_{p,r} + c_s C_{p,s})(T_f - T) \quad (32)$$

Enthalpy is conserved in the reactor, so the system comprising eqs 31 and 32 should have a first integral. It can be shown that eqs 31 and 32 can be expressed in the form

$$V\frac{d\phi}{dt} = -F\phi \quad (33)$$

By explicitly using the relation 30 in eq 27 we may write, before differentiation,

$$V\frac{d}{dt}[cC_{p,r} + (c_f - c)(C_{p,p} + c_s C_{p,s})(T - T_f) - (h_p - h_r)(c - c_f)] = -F[(c_f C_{p,r} + c_s C_{p,s})(T - T_f) - (h_p - h_r)(c - c_f)] \quad (34)$$

which has the required form if we can show that

$$cC_{p,r} + (c_f - c)C_{p,p} = c_f C_{p,r} \quad (35)$$

A simple thermodynamic argument suffices. Invoking relation (28) once more gives

$$c\frac{dh_r}{dT} + c_f\frac{dh_p}{dT} - c\frac{dh_p}{dT} = c_f\frac{dh_r}{dT} \quad (36)$$

from which we find that

$$(c_f - c)\,dh_p = (c_f - c)\,dh_r \quad (37)$$

Thus $h_p = h_r$ + constant, and our case is proved. The enthalpy balance (eq 32) may now be rewritten

$$V\bar{C}\frac{dT}{dt} = (-\Delta H)Vcze^{-(E/RT)} + F\bar{C}(T_f - T) \quad (38)$$

where the $\bar{C}$ is a volumetric specific heat of the feed mixture, weighted for the relative concentrations of reactant and solvent. It can be seen that the use of two separate reaction mixture specific heats in eq 4 of section 2 is probably unnecessary. The inclusion of a heat loss rate with a constant coefficient, a mechanical work term, or a solid mass capacitance parameter does not alter this result.

Literature Cited

Andronov, A. A.; Leontovich, E. A.; Gordon, I. I.; Maier, A. G. *Theory of Bifurcations of Dynamic Systems on a Plane*; Israel Program for Scientific Translations Ltd.: Jerusalem, London, 1973.

Aris, R.; Amundson, N. R. An Analysis of Chemical Reactor Stability and Control—I. The Possibility of Local Control, with Perfect or Imperfect Control Mechanisms. *Chem. Eng. Sci.* **1958**, *7*, 121–131.

Balakotaiah, V.; Luss, D. Multiplicity Features of Reacting Systems: Dependence of the Steady States of CSTR on the Residence Time. *Chem. Eng. Sci.* **1983**, *38*, 1709–1721.

Bilous, O.; Amundson, N. R. Chemical Reactor Stability and Sensitivity. *AIChE J.* **1955**, *1*, 513–521.

Brengel, D. D.; Seider, W. D. Coordinated Design and Control Optimization of Nonlinear Processes. *Comput. Chem. Eng.* **1992**, *16*, 861–886.

Chang, M.; Schmitz, R. A. An Experimental Study of Oscillatory States in a Stirred Reactor. *Chem. Eng. Sci.* **1975a**, *30*, 21–34.

Chang, M.; Schmitz, R. A. Feedback Control of Unstable States in a Laboratory Reactor. *Chem. Eng. Sci.* **1975b**, *30*, 837–846.

Denbigh, K. G.; Turner, J. C. R. *Chemical Reactor Theory: an Introduction*, 2nd ed.; Cambridge University Press: New York, 1971.

Furusawa, T.; Nishimura, H.; Miyauchi, T. Experimental Study of Bistable Continuous Stirred-Tank Reactor. *J. Chem. Eng. Jpn.* **1969**, *2* (1), 95–100.

Golubitsky, M.; Keyfitz, B. L. A Qualitative Study of the Steady-State Solutions for a Continuous Flow Stirred Tank Chemical Reactor. *SIAM J. Math. Anal.* **1980**, *11*, 316–339.

Golubitsky, M.; Schaeffer, D. G. *Singularities and Groups in Bifurcation Theory*; Springer-Verlag: New York, 1985; Vol. 1.

Gray, B. F. Analysis of Chemical Kinetic Systems Over the Entire Parameter Space III. A Wet Combustion System. *Proc. R. Soc. London A* **1990**, *429*, 449–458.

Gray, B. F.; Roberts, M. J. A Method for the Complete Qualitative Analysis of two Coupled O.D.E.'s Dependent on Three Parameters. *Proc. R. Soc. London A* **1988a**, *416*, 351–389.

Gray, B. F.; Roberts, M. J. Analysis of Chemical Kinetic Systems Over the Entire Parameter Space I. The Salnikov Thermokinetic Oscillator. *Proc. R. Soc. London A* **1988b**, *416*, 391–402.

Gray, B. F.; Roberts, M. J. Analysis of Chemical Kinetic Systems Over the Entire Parameter Space II. Isothermal Oscillators. *Proc. R. Soc. London A* **1988c**, *416*, 403–424.

Gray, B. F.; Forbes, L. K. Analysis of Chemical Kinetic Systems Over the Entire Parameter Space IV. The Salnikov Oscillator With Two Temperature-Dependent Reaction Rates. *Proc. R. Soc. London A* **1994**, *444*, 621–642.

Gray, B. F.; Coppersthwaite, D. P.; Griffiths, J. F. A Novel, Thermal Instability in a 'Semi-Batch' Reactor. *Process Saf. Prog.* **1993**, *12* (1), 49–54.

Heemskerk, A. H.; Fortuin, J. M. H. The Hysteresis of Steady States in a Grandientless Liquid-Phase Reaction System. *Chem. Eng. Sci.* **1983**, *38*, 1261–1269.

Heemskerk, A. H.; Dammers, W. R.; Fortuin, J. M. H. Limit Cycles Measured in a Liquid-Phase Reaction System. *Chem. Eng. Sci.* **1980**, *35*, 439–445.

Hlavacek, V.; Kubicek, M.; Jelinek, J. Modeling of Chemical Reactors—XVIII. Stability and Oscillatory Behaviour of the CSTR. *Chem. Eng. Sci.* **1970**, *25*, 1441–1461.

Lewin, D. R.; Lavie, R. Designing and Implementing Trajectories in an Exothermic Batch Chemical Reactor. *Ind. Eng. Chem. Res.* **1990**, *29*, 89–96.

Marsden, J. E.; McKracken, M. *The Hopf Bifurcation and its Applications*; Springer-Verlag, Berlin, 1976.

Ray, W. H.; Hastings, S. P. The Influence of the Lewis Number on the Dynamics of Chemically Reacting Systems. *Chem. Eng. Sci.* **1980**, *35*, 589–595.

Schmitz, R. A.; Bautz, R. R.; Ray, W. H.; Uppal, A. The Dynamic Behaviour of a CSTR: Some Comparisons of Theory and Experiment. *AIChE J.* **1979**, *25*, 289–297.

Seider, W. D.; Brengel, D. D.; Provost, A. M.; Widagdo, S. Nonlinear Analysis in Process Design: Why Overdesign to Avoid Complex Nonlinearities. *Ind. Eng. Chem. Res.* **1990**, *29*, 805–818.

Uppal, A.; Ray, W. H.; Poore, A. B. On the Dynamic Behaviour of Continuous Stirred Tank Reactors. *Chem. Eng. Sci.* **1974**, *29*, 967–985.

Vaganov, D. A.; Samoilenko, N. G.; Abramov, V. G. Periodic Regimes of Continuous Stirred Tank Reactors. *Chem. Eng. Sci.* **1978**, *33*, 1133–1140.

Van Heerden, C. The Character of the Stationary State of Exothermic Processes. *Chem. Eng. Sci.* **1958**, *8*, 133–145.

Vejtasa, S. A.; Schmitz, R. A. An Experimental Study of Steady State Multiplicity and Stability in an Adiabatic Stirred Reactor. *AIChE J.* **1970**, *16*, 410–419.

Vermeulen, D. P.; Fortuin, J. M. H. Experimental Verification of a Model Describing the Transient Behaviour of a Reaction System Approaching a Limit Cycle or a Runaway in a CSTR. *Chem. Eng. Sci.* **1986**, *41*, 1089–1095.

Vermeulen, D. P.; Fortuin, J. M. H.; Swenker, A. G. Experimental Verification of a Model Describing Large Temperature Oscillations of a Limit-Cycle Approaching Liquid-Phase Reaction Systems in a CSTR. *Chem. Eng. Sci.* **1986**, *41*, 1291–1302.

Received for review December 20, 1994
Revised manuscript received June 20, 1995
Accepted July 6, 1995[⊗]

IE9407520

[⊗] Abstract published in *Advance ACS Abstracts,* October 1, 1995.